Generation, Detection and Characterization of Photonic Quantum States

a dissertation report

Ivo Straka

Faculty of Science | Palacký University

Olomouc
2019

Title:	Generation, Detection and Characterization of Photonic Quantum States
Author:	Mgr. Ivo Straka
ORCID:	0000-0003-2675-6335
ResearcherID:	V-2610-2017
Advisor:	prof. Mgr. Jaromír Fiurášek, Ph.D.
Consultant:	RNDr. Miroslav Ježek, Ph.D.
Ph.D. programme:	Optics and Optoelectronics (full-time form)
Institution:	Department of Optics, Faculty of Science, Palacký University
Year:	2019
Pages:	33
External Examiners:	Aurél Gábris, Ph.D. *FJFI ČVUT, Prague* prof. RNDr. Tomáš Opatrný, Dr. *PřF UP, Olomouc*

The thesis is available for reading at the study department of the Faculty of Science, Palacký University, 17. listopadu 12, Olomouc. It is also available online at stag.upol.cz under Browse and Theses. The personal number is R12978.

Abstract

This report presents the main results of the thesis titled Generation, Detection and Characterization of Photonic Quantum States.

The presented results compare quantum non-Gaussian properties of single-photon states produced by optical frequency conversion and radiative recombination in a quantum dot. The primary concern is resilience against optical loss that is inevitable in all real applications. Quantum non-Gaussianity is also measured using multiphoton states composed of multiple heralded single photons generated by frequency conversion. Another quantum property is genuine n-photon quantum non-Gaussianity, which is investigated using multiphoton states with respect to optical loss and added noise.

Furthermore, the thesis presents a method of programmable intensity modulation as a source of arbitrary classical photon statistics. The method includes calculation of the respective intensity distribution.

The procedures employed in the thesis include constructing a source of correlated photons based on frequency down-conversion. The source was used to obtain the results pertaining to multiphoton quantum non-Gaussianity. Next, a counting model of single-photon avalanche diodes is developed, both analytically and in simulation. These results were used in measuring arbitrary photon statistics.

Keywords: quantum optics, photon statistics, quantum non-Gaussianity

Acknowledgements

I thank Miroslav Ježek for his invaluable mentoring, ideas, diligence, and for all his hard work put into the Quantum Optics Lab, its projects and its team. Without him, this thesis would never have been written. I am also grateful to Jaromír Fiurášek for his guidance and constant support during my studies. I thank Radim Filip for his ideas, discussions and for our common projects. I am thankful to the whole QOLO team for their help and for maintaining a friendly and open atmosphere; with special thanks to Martina Miková/Nováková for her unceasing assistance, support, and nourishment. I am grateful to all my senior colleagues in the department for their hard work and making sure that the possibilities the students have are constantly growing. I thank all the collaborators I have not yet named with special thanks to Ana Predojević for her work on onions, Quantera, and for keeping it real. I thank our administrative team for making everything work. I am especially grateful to all my friends I met at the department for their company and I thank the Derkach family for being so awesome. My special thanks belong to my friends the musicians and to the Lindy community who have kept me sane all these years and always relieved me of the work-related stress and guilt. A very special thanks goes to my family, to whom I owe more than I could say here.

Contents

Preface

The thesis that is the subject of this report is the result of my post-graduate studies at the Department of Optics at Palacký University. Its aim is to present new advances in witnessing quantum properties of light and generating arbitrary classical photon statistics. The thesis is based on four publications denoted in References under A1, A2, A3, and A4. The first three have been peer-reviewed and published, while the last one is under peer review at the time of writing. Here I aim to explain my involvement and contribution to the presented work.

The experimental research into quantum non-Gaussianity began during my master's studies under the supervision of Miroslav Ježek.[1] The subject of the thesis was building a down-conversion source, which was incidentally used to measure the data for the publication 2.

The research continued during the first year of my post-graduate studies under Miroslav, when I visited the group of professor Gregor Weihs. In the mutual collaboration of the theoreticians and experimentalist of our department in Olomouc, professor Weihs' group in Innsbruck and professor Glenn Solomon in Gaithersburg, quantum

non-Gaussianity of multiple single-photon sources was evaluated.[A1] I was responsible for measuring the continuous-wave down-conversion data and during my stay in Innsbruck, I worked with Lorenz Butschek to measure the pulsed down-conversion data. I was also responsible for writing the appropriate parts, synthesis of the results, editing the manuscript and the submission process.

The project that followed is not included in this thesis. It was focused on bipartite entanglement localisation with respect to the temperature of an incoherent environment (I. Straka, M. Miková, M. Mičuda, M. Dušek, M. Ježek, R. Filip, Sci. Rep. 5, 16721, year 2015).

Lukáš Lachman and Radim Filip then developed a hierarchy of quantum non-Gaussian criteria that we experimentally tested on a new down-conversion source.[A2] My task was to construct the source, perform the measurement and process the data. I was also responsible for writing the appropriate parts, editing the manuscript and handling all submissions. The results are considered theoretical and experimental by equal part, with Lukáš and I being the graduate students chiefly responsible for the respective parts.

The last work on genuine quantum non-Gaussianity utilized the same multichannel measurement scheme as the previous project.[A4] My contribution again concerned the source, measurement, data processing and writing the experimental part, while editing and submission of the manuscript was the responsibility of Lukáš.

The last presented project started as an idea of Miroslav Ježek that was developed by Jaromír Mika in his bachelor's and master's thesis under my supervision.[3] Afterwards, Miroslav and I continued the work to produce a publication.[A3] I was responsible for building the setup, developing the numerical and driving methods, formulating the detection model and calibrating the detectors, measuring and processing the data, and writing the chief part of the manuscript.

All of the presented work was supervised by Miroslav Ježek, who has been closely involved in all experimental and technical work, analyses of the data, discussions and writing. I feel that his invaluable work and close involvement with my contributions should be acknowledged here as well.

At the time of writing I can be contacted via the electronic addresses below. I welcome any feedback or questions that the reader may have; if only for the joy of someone reading my thesis.

Olomouc
March 2019

Ivo Straka
ivo.straka@gmail.com
straka@optics.upol.cz

1 Introduction

This report presents the main results of the dissertation titled Generation, Detection and Characterization of Photonic Quantum States. It presents advances in recognizing quantum non-Gaussian photonic states and in manipulating the photon statistics to suit a predefined distribution.

Section 2 describes the experimental realization of a source of correlated photons. This source is used to generate heralded single photons in sections 5 and 6. Section 3 provides the description of single-photon avalanche diodes that are used as detectors. Their detailed description is needed particularly for verifying custom-generated photon statistics in section 7. The section offers ways of modelling the detectors' response to photon statistics. Section 4 presents measurements of non-Gaussian light produced on various physical platforms and its resilience against loss.[A1] Section 5 tests a new way of recognizing QNG that is optimized for multiphoton states.[A2] Section 6 demonstrates witnessing of a more specialized quantum property called *genuine* quantum non-Gaussianity that distinguishes non-Gaussian presence of a certain number of photons.[A4] Finally, section 7 practically treats the problem of generating arbitrary photon statistics.[A3]

2 SPDC source of photon pairs

This SPDC source was used in the experiments described in section 5 and published in references A2 and A4. Moving this source to a mobile breadboard, including reassembling and alignment, was the subject of a bachelor's thesis by M. Neset.[4]

The source is based on collinear type-II down-conversion in a periodically poled $KTiOPO_4$ crystal (ppKTP). The crystal is 6 mm thick and comprises of three poling domains, each approximately 1×1 mm wide. The poling periods are 9.900, 10.000, and 10.075 μm. The middle domain is used, as it offers optimal temperature tuning for the pump at 405 nm. The optical setup is shown in Figures 1 and 2.

The experiment generates temporally correlated photon pairs that can be used a heralded single-photon source. The two-photon interference[5] is shown in Figure 3. The corresponding biphoton spectral amplitude is shown in Figure 4.

3 Single-photon avalanche diodes (SPAD)

This section provides a general description of single-photon avalanche diodes[B1] and develops counting models that describe their operation.

SPADs are semiconductor avalanche diodes operated with a reverse voltage that is above the breakdown voltage. Upon an absorption of a photon, an electron-hole pair

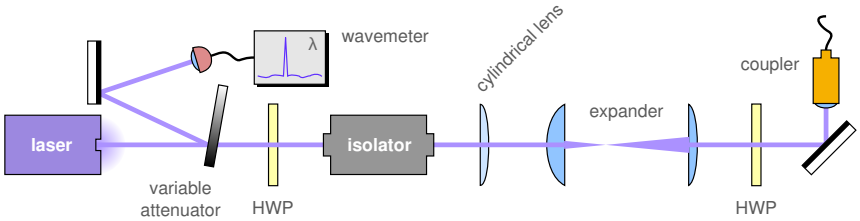

Figure 1: Continuous-wave laser diode at 405 nm is used as pump. A rotational reflective attenuator serves for adjusting pump power, while the reflected beam is coupled into a wavemeter. An isolator prevents any reflections from entering the laser. A half-wave plate (HWP) rotates the polarization to match the isolator and maximize transmission. Ellipticity of the beam is corrected using a 200-mm cylindrical lens and two spherical lenses that serve as an expander (50 mm and 125 mm). Before coupling, a HWP rotates the polarization so that it matches the slow axis of a polarization-maintaining fibre.

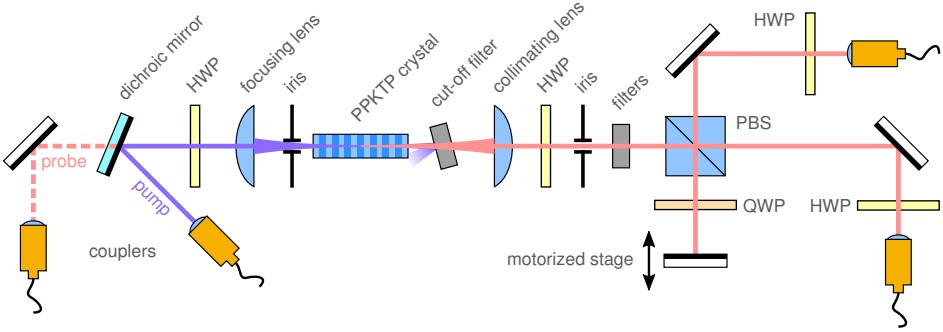

Figure 2: The type-II collinear SPDC source using a periodically poled KTP crystal with a 10 µm poling period. All optical inputs and outputs are coupled in single-mode polarization-maintaining fibres. All components before the crystal are designed and coated for the pump wavelength 405 nm; all components afterwards are for 810 nm (the faces of the crystal are dual-band AR-coated). A dichroic mirror allows a probing beam at 810 nm to enter the setup. The linear polarization of the pump is rotated using a half-wave plate (HWP) onto a vertical polarization. A 100-mm lens provides focusing into the nonlinear crystal. Afterwards, a cut-off filter removes most of the pump. The down-converted signal and idler are collimated using a 150-mm lens. A HWP is used for alignment and to match the frame of reference of the crystal to the polarizing beam splitter (PBS). Further cut-off and band-pass filtering is carried out using additional filters. The PBS separates signal and idler into two arms. One of them goes through a delay line, where a motorized mirror serves as a back-reflector. A double pass through a quarter-wave plate (QWP) makes sure that the delayed beam is transmitted through the PBS into the top arm. HWPs in front of the fibre couplers serves to match the linear polarizations with slow-axis modes of the fibres.

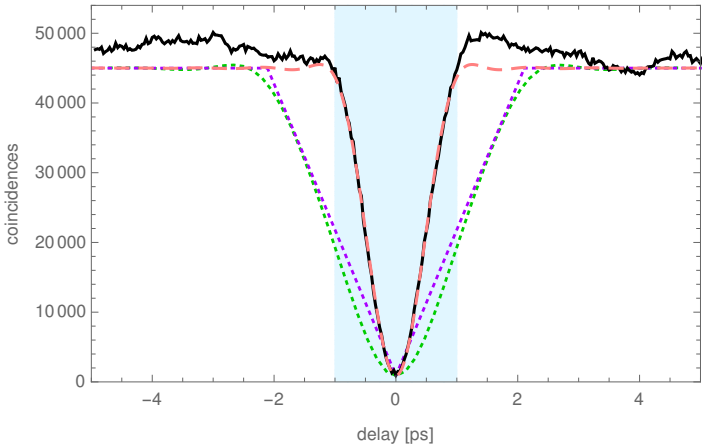

Figure 3: The Hong-Ou-Mandel dip. The black curve represents the data and their statistical error. The drift comes from systematic errors, most likely pump stability. HOM visibility = 98.9 ± 0.2 % from data; the best fit of the models is 98 %. A perfect sinc-spectrum dip is shown by the triangular purple dotted curve. Further augmentation by a band-pass filter is estimated by the green dotted curve. The red dashed curve represents the numerical model based on the interpolated spectral profile presented in Figure 4. The light-blue region designates the data range that was the basis of the numerical model.

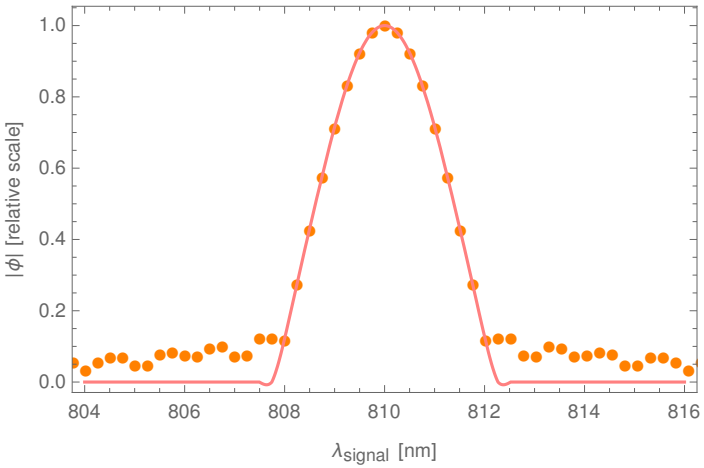

Figure 4: The joint spectral amplitude numerically calculated from the HOM data. The wavelengths are approximately correlated by $(\lambda_{\text{signal}} + \lambda_{\text{idler}})/2 \approx 810$ nm. Orange dots are the numerical result and the red line is the interpolation of the central peak with side-artefacts cleaned up.

may be excited in the p-n junction of the diode. The work presented in this theses utilizes silicon SPADs, which have optimal efficiency in the visible spectrum. All detected signals were at 810 nm, where the typical efficiency of detecting a photon is 50–70 %.

Important aspects of SPADs include their temporal properties. The recovery time τ_R is a time period after each detection, when the SPAD is unable to detect another photon. The relative time uncertainty of the output signal is called jitter, which is commonly defined as a FWHM of the detection-to-output time distribution. Typical values for detectors in this work are in the order of fractions of a nanosecond. Dark counts represent the ocurrence rate of background detections present without any incident signal. Values depend on the type of the SPAD and its age, in this work typically 10–500 counts per second. Another type of false counting arises from carriers trapped in energy levels close to the conduction band that represent impurities in the material. After quenching and recovery, these carriers may cause an avalanche by themselves, resulting in a so-called afterpulse. Afterpulsing is expressed by a probability of occurrence p_a and a temporal distribution. Photons arriving during recovery time also contribute to afterpulsing, because the unquenched carriers they excite may cause an avalanche immediately after the reverse voltage is applied. This adds to p_a a factor that grows linearly with the incident light intensity. In the literature, these events are referred to as twilight pulses.

The following model presents modelling the probability distribution of the number of detections in a fixed time window; usually referred to as counting statistics. The basis of the model is a homogeneous Poisson point process[B2] that is modified by considering basic detector imperfections – recovery time and afterpulses.[B1] Let us work with interarrival time $\Delta t = \tau_R + t$, which is the time interval between two successive detections. The stochastic part t has the probability density function

$$P(t) = \alpha\lambda\delta(t) + a\left[e^{-\lambda t}\, p_{\mathrm{AP}}(t) + (1 - \widetilde{p}_{\mathrm{AP}}(t))\lambda e^{-\lambda t}\right] + (1 - a - \alpha\lambda)\lambda e^{-\lambda t}. \quad (1)$$

This model can be used to numerically simulate data for any event rate λ. It was used to provide all theoretical predictions of photon-number distributions that are used in Chapter 7. Calibration results are shown in Figure 5.

The model also establishes an analytical correction for saturation of the detector due to afterpulsing and dead time. The mean detection rate is

$$\lambda_{\mathrm{det}} = \left(\frac{1}{\lambda} - \frac{a}{\lambda}\int_0^\infty p_{\mathrm{AP}}(t)\, e^{-\lambda t}\, \mathrm{d}t + \tau_R - \alpha\right)^{-1}. \quad (2)$$

The required parameters τ_R, a, α and $p_{\mathrm{AP}}(t)$ can be established by direct measurements. To obtain an analytical expression, the model needs to be simplified to immediate afterpulsing with probability p_a,

$$p_{\mathrm{inter}}(t) = p_a\delta(t) + (1 - p_a)\lambda e^{-\lambda t}, \quad t \geq 0. \quad (3)$$

The counting distribution is then

$$P_0(T) = \frac{1-p_a}{1-p_a+\lambda\tau_R} e^{-M_1}, \tag{4}$$

$$\begin{aligned} P_{0<n<N}(T) = {} & \frac{1}{1-p_a+\lambda\tau_R} \\ & \times \sum_{k=0}^{n} \binom{n}{k} p_a^{n-k}(1-p_a)^k \Big[(k+1-p_a) Q_{k+1}^{n+1} \\ & - M_{n+1} Q_k^{n+1} - \Big(2k + (1-k/n)(1-p_a)\Big) Q_{k+1}^{n} \\ & + (p_a k/n + 2M_n) Q_k^n + k\, Q_{k+1}^{n-1} - (k/n + M_{n-1}) Q_k^{n-1} \Big], \end{aligned} \tag{5}$$

$$\begin{aligned} P_N(T) = {} & \frac{1}{1-p_a+\lambda\tau_R} \Bigg\{ -M_0 \\ & + \sum_{k=0}^{N} \binom{N}{k} p_a^{N-k}(1-p_a)^k \Big[(p_a k/N + 2M_N) Q_k^N \\ & - \Big(2k + (1-k/N)(1-p_a)\Big) Q_{k+1}^{N} + k\, Q_{k+1}^{N-1} \\ & - (k/N + M_{N-1}) Q_k^{N-1} \Big] \Bigg\} + N + 1, \end{aligned} \tag{6}$$

$$\begin{aligned} P_{N+1}(T) = {} & \frac{1}{1-p_a+\lambda\tau_R} \Bigg\{ M_0 \\ & + \sum_{k=0}^{N+1} \binom{N+1}{k} p_a^{N+1-k}(1-p_a)^k \Big[k Q_{k+1}^{N} \\ & - \left(\frac{k}{N+1} + M_N \right) Q_k^N \Big] \Bigg\} - N, \end{aligned} \tag{7}$$

where the terms M and Q are

$$M_n \coloneqq \lambda(T - n\tau_R), \tag{8}$$

$$Q_k^n \coloneqq Q_k(M_n) = \begin{cases} 0 & \text{if } k = 0 \\ e^{-M_n} \sum_{i=0}^{k-1} M_n^i / i! & \text{if } k \geq 1 \end{cases}, \tag{9}$$

using parameters λ (incident rate), p_a (probability of an afterpulse) and τ_R (recovery time). The number of detections where the analytical expression changes is $N = \lfloor T/\tau_R \rfloor$.

In the limit of $p_a \to 0$, or $p_a \equiv 0$ if one postulates $0^0 := 1$, the relations are reduced to the form published by Müller for a dead-time-only process (equations (32)).[6] To capture twilight pulsing, p_a can be made a function of λ.

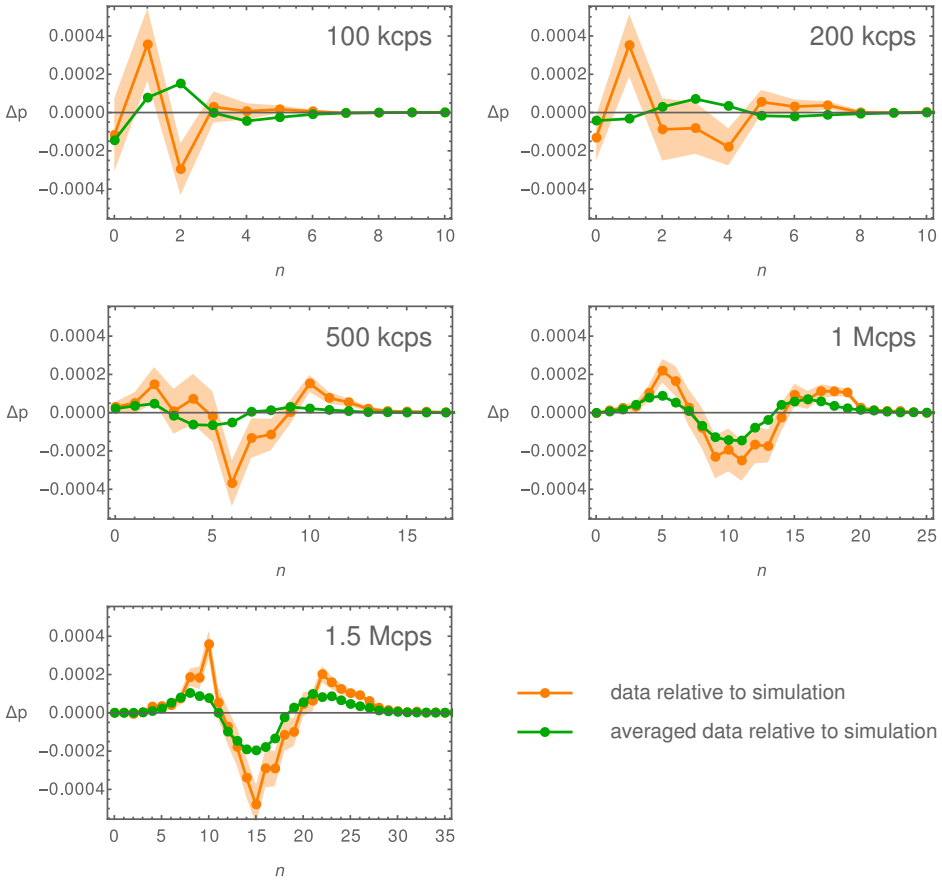

Figure 5: The detector model compared to measured data for a constant intensity. The differences in photon-number probabilities between data and a numerical simulation of model (1) are plotted in orange including statistical errors of the data. Green points represent simulated data that share the same interarrival time statistics with the measured data. This averages out any fluctuations and for a homogeneous point process, both curves should be identical. However, green points are generally closer to zero than orange points, which suggests the presence of fluctuations either in the signal or in the behaviour of the detector. The parameters of the model were $\tau_R = 23$ ns, $a = 0.0235$, $\alpha = 2$ ns, and λ was taken so that the mean number of detections was the same as in the data. The model is shown to be accurate with deviations in the order of 10^{-4}.

4 Quantum non-Gaussian light

This section is based on the publication by Straka and colleagues (2014).[A1]

Photonic Fock states[B3] represent an essential resource that allows harnessing the quantum properties of light. There are several quantum characteristics that such states possess that can be experimentally recognized. Nonclassical states, by definition, go beyond the description of classical optical theory. Any state that cannot be expressed as a statistical mixture of coherent states (displaced vacuum states) is nonclassical.[7,8] One can go a step further and consider a convex mixture of Gaussian states (squeezed and displaced vacuum states). A quantum state incompatible with any such mixture is quantum non-Gaussian.[9]

Quantum non-Gaussianity (QNG) is a quantum property that can be recognized in single photons that exhibit a positive Wigner function. There are several ways of witnessing this property[2,9–13] and it has been positively recognized on a number of physical systems.[2,14–16] This work follows the experimental proof by Ježek and colleagues[2] by exploring the properties of QNG depth for various physical platforms. Single photons were produced by frequency conversion of continuous and pulsed light, and recombination of excitons in a semiconductor quantum dot. The split-detector approach allows estimation of a lower bound on the QNG depth.

The QNG witness approximation was formulated by Lachman and Filip.[A1] In the Fock basis, let P_n denote the probability of n photons. Let $P_{2+} = 1 - P_0 - P_1$ quantify the undesirable multi-photon contribution. The idea of the QNG witness is to conservatively estimate P_1 and P_{2+} so that they unequivocally prove QNG by passing extremal values of Gaussian mixtures.[2] Such a threshold can be expressed parametrically,[2] but in the limit of a lossy, high-quality single photon sources $P_{2+} \ll P_1 \lesssim 0.1$ an approximation can be used,[17]

$$P_{2+} < \frac{2}{3} P_1^3. \tag{10}$$

A nonclassicality condition in the same approximation is $P_{2+} < \frac{1}{2} P_1^2$, which is less strict.[18] To analytically evaluate the QNG depth, the approximation $P_{2+} \approx P_2 \ll P_1$ is used. The subsequent transmittance necessary to preserve QNG is then bounded by

$$T > \frac{3}{2} \frac{P_{2+}}{P_1^3}. \tag{11}$$

This proves to be a good estimate for the QNG depth for realistic single photon sources, as evident from the presented data. This figure can be also directly measured using attenuation in the experiment.

In this work, three different systems were used to generate single-photon states. Of these, two were based on spontaneous parametric down-conversion (SPDC) in a nonlinear crystal. The third system was an InAs/GaAs single quantum dot.

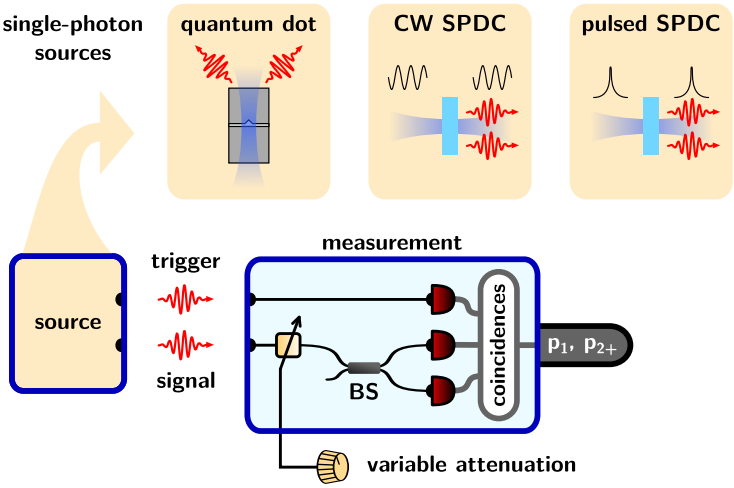

Figure 6: The autocorrelation measurement scheme. A single-photon state is heralded by the trigger photon and subjected to attenuation. p_1 and p_{2+} are estimated using the Hanbury Brown–Twiss setup.[2]

The first SPDC source (located in Olomouc) was based on a 2-mm-thick BBO crystal in a type-II collinear configuration that was operated in the continuous-wave (cw) regime. Here, the pump power was 90 mW while its wavelength was 405 nm. Correlated photons were spectrally filtered to a bandwidth of 2.7 nm.[1,2] The second SPDC source (located in Innsbruck) produced entangled photon pairs. It contained a 15-mm-long type-II ppKTP nonlinear crystal embedded in a Sagnac-type interferometer loop.[19] This source was pumped by a 2-ps pulsed laser light of 404 nm wavelength and 80 μW power per loop direction. The quantum dot sample contained low density self-assembled InAs/GaAs quantum dots embedded in a planar microcavity. The excitation light was derived from a tunable Ti:sapphire laser that could be operated in picosecond-pulsed (82 MHz repetition rate) or continuous-wave mode.[20] Two data sets were generated with this system, one in resonant two-photon excitation using the pulsed mode and the other in above-band continuous-wave mode.

The measurement scheme was a triggered autocorrelation shown in Figure 6. Variable attenuation was introduced by moving a blade in the beam. Data acquisition was carried out by a time-to-digital converter which stored arrival times of every detection event. The trigger detector conditioned the detections in the signal arm: any detection within a coincidence time window centred around a trigger detection was considered a coincidence. From these, the probabilities p_0, p_1, p_{2+} were calculated, which are estimators of P_0, P_1, P_{2+}.[2] These parameters allow constructing the witnesses for NC and QNG states.

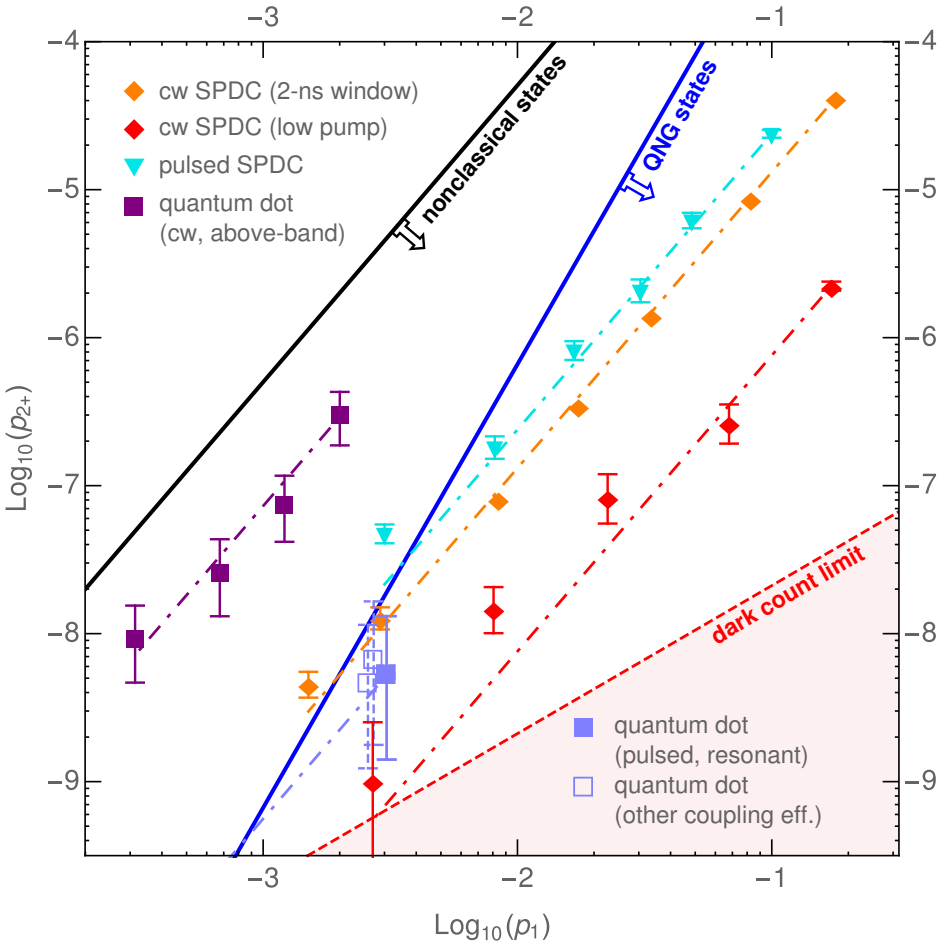

Figure 7: Estimated probabilities of heralded single-photon states on a log-log scale. Each series represents various attenuations of a particular state. Full diamonds denote the cw SPDC source: orange – coincidence window 2 ns; red – low pump, coincidence window 2 ns. Cyan triangles denote the pulsed SPDC source. Square markers denote the quantum dot: purple squares – above-band excitation, cw pump; blue squares – resonant excitation, pulsed pump. The dot-dashed lines represent theoretical prediction of attenuation from the initial point. The dashed red line is the limit of dark counts for the red attenuation data. The solid black and blue lines represent NC and QNG witnesses, respectively. Error bars in this figure have been slightly changed with respect to the presentation in reference A1, where a naïve approach was mistakenly used. The change is, however, cosmetic and the results remain unchanged. Here, error bars represent Bayesian 68%-confidence intervals stemming from statistical counting errors. Horizontal error bars are smaller than plot points.

In Figure 7, the measurement results obtained from all three single-photon sources are compared. For the pulsed SPDC source (cyan triangles) the estimated QNG depth is 14.5 dB; the experimentally confirmed value is 10.8 dB. The cw SPDC source measured with 2-ns coincidence window (orange diamonds) yields a theoretical depth of 19.6 dB and a proven depth of 17.9 dB. Red diamonds also stand for the cw SPDC, but with reduced pump power to bring down multi-pair contributions to a level comparable with the quantum dot source. The expected depth is 31.8 dB while the measured value is 18 dB. The most attenuated state also visibly approaches the dark count limit of the detectors and so, further attenuation would be meaningless. The state generated by a quantum dot excited above-band (purple squares) shows only nonclassicality and cannot be well compared to SPDC states. With resonant pulsed excitation (blue square), the quantum dot state exhibits QNG character and the theoretical depth is 5.6 dB. Empty blue squares show additional quantum dot states measured with different collection efficiencies. However, in order to measure the QNG depth directly here, the measurement time here would exceed the stability of the system.

5 Multiphoton states

This section is based on the publication by Straka, Lachman, and colleagues (2018).[A2]

The QNG criterion discussed in the previous chapter is universal for all quantum states, however it is suitable primarily for recognizing QNG in single-photon states. In this chapter, a multichannel detection scheme will be used to conveniently recognize QNG in multiphoton states.

The detector splits incoming light evenly to multiple separate single-photon binary detectors, as depicted in Figure 8. The detector has $n+1$ channels, from which n particular channels are selected. Let us denote the probability of coincident detections on these channels R_n. The probability of all channels registering photons is R_{n+1}. For light with small mean number of photons, the sufficient condition for QNG can be approximated by

$$(R_n)^{n+2} > H_n^4(x)\left[\frac{R_{n+1}}{2(n+1)^3}\right]^n, \tag{12}$$

where $H_n(x)$ is the maximum value of a Hermite polynomial among such values of $x : H_{n+1}(x) = 0$.

Multiphoton states were produced by mixing n single-photon states together incoherently using time multiplexing. The resulting multi-mode state is subjected to condition 12, where all detectors are considered binary within the measurement window. The source of single photons is described in section 2. The heralding rate was set to about 650 kHz, which corresponds to the maximum data flow allowed by the coincidence electronics. n successive time windows were taken, in which a single photon was

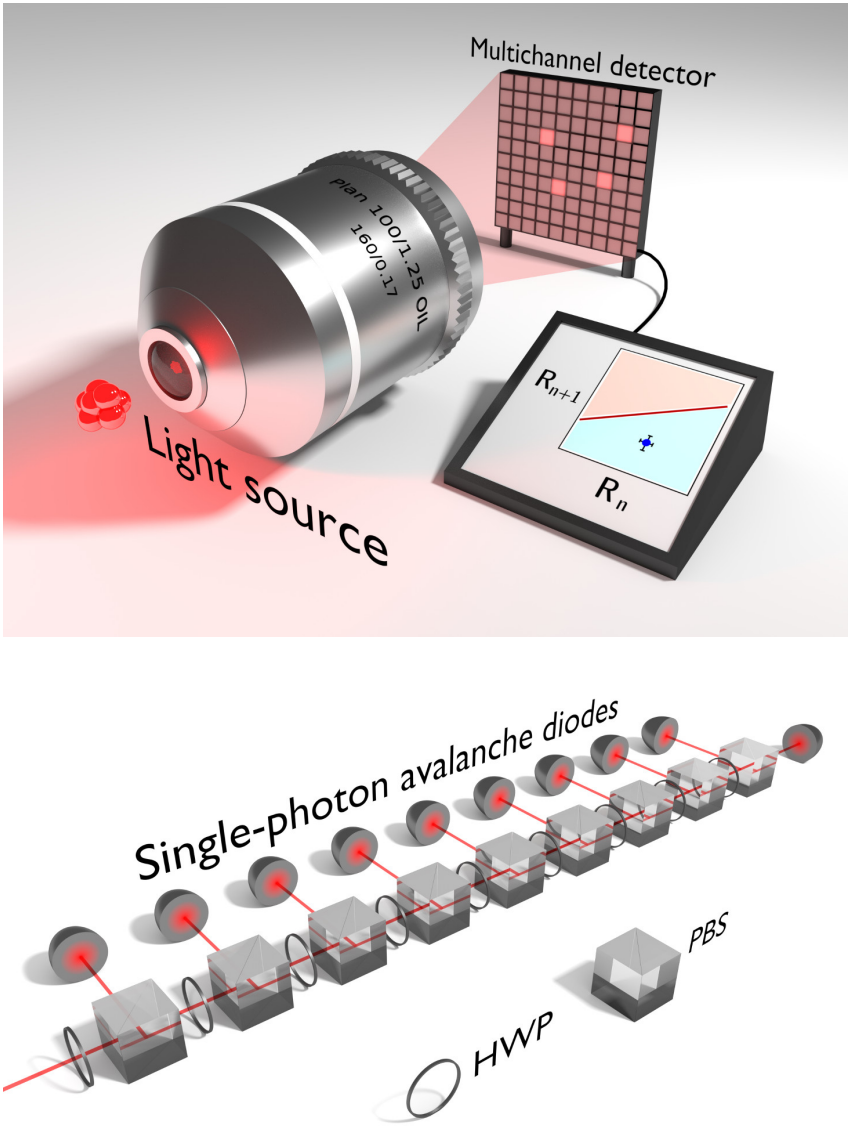

Figure 8: A general proposal of the experimental QNG witness. **Top:** multiphoton light is collected and brought to a balanced multichannel detector, where coincidences R_n, R_{n+1} are compared to the QNG threshold. **Bottom:** the detector consists of 10 silicon single-photon avalanche diodes (SPAD) and a balanced array of polarizing beam splitters (PBS) and half-wave plates (HWP) to control the splitting ratio. The half-wave plates can be adjusted to split the light equally to any number of selected channels, so there is no need to physically add or remove SPADs.

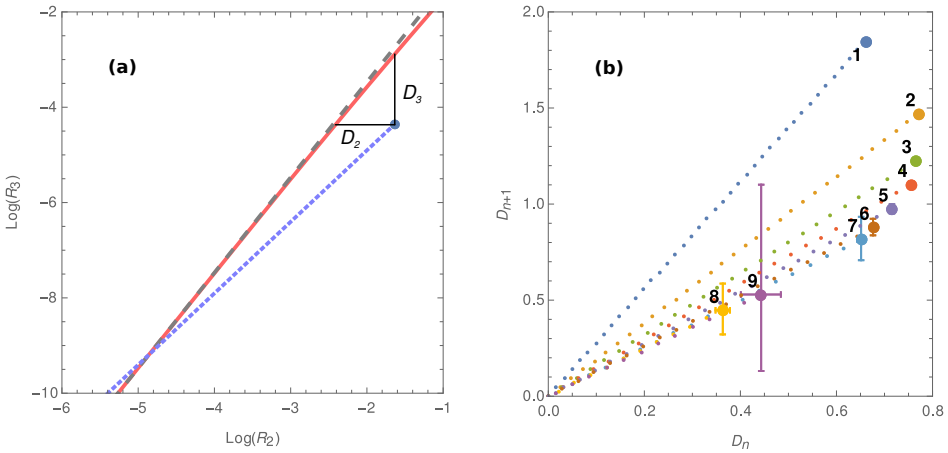

Figure 9: QNG tests for heralded 1-9 photons. **(a)** Example for $n = 2$. Red line represents the QNG criterion, while dashed grey line is its approximation (12). The blue point represents the measured state and the dotted blue line is the path of the point if the state becomes further attenuated. For the sake of visualising attenuation for all data, let us denote D_n, D_{n+1} as the horizontal and vertical log-distances between a measured point and the QNG threshold. **(b)** The distances D_n and D_{n+1} are plotted for measured points as well as for predicted attenuations. Reaching the point of origin at zero means that QNG is no longer recognizable. Dotted paths represent attenuation with steps of 0.5 dB per dot. Note that these steps are not the same size for all n. The number of steps on each path is proportional to QNG depth. For QNG depth values, see Figure 10.

heralded, and were joined into a single temporal detection unit. The positions of these respective time windows were heralded by a detector in one of the SPDC modes.

A multichannel detector was built by Josef Hloušek; a network of polarizing beam splitters and half-wave plates to construct a balanced 1-to-$(n + 1)$ splitter. The design is equivalent to the one depicted in Figure 8, but a tree structure was used instead of a linear one. In each arm, a silicon single-photon avalanche diode (SPAD) was placed as a detector. Even though each SPAD has different efficiency, it is sufficient to adjust the beam splitter network so that the responses of all detectors are balanced. This way, the measured state is merely subjected to additional loss, but that does not create any false positives in QNG witnessing.[2] The total number of channels was 10; one SPAD was additionally used as a heralding detector.

Data acquisition employed two time-to-digital converters, each having 8 channels with the resolution of 81 ps/time bin. Since 11 channels were needed in total, two modules were used and synchronized with a shared periodic signal at 100 kHz. This frequency was chosen to compensate the measured relative clock drift 10^5 time bins/second.

The estimated mean numbers of photons were up to 5, if the detector efficiency is

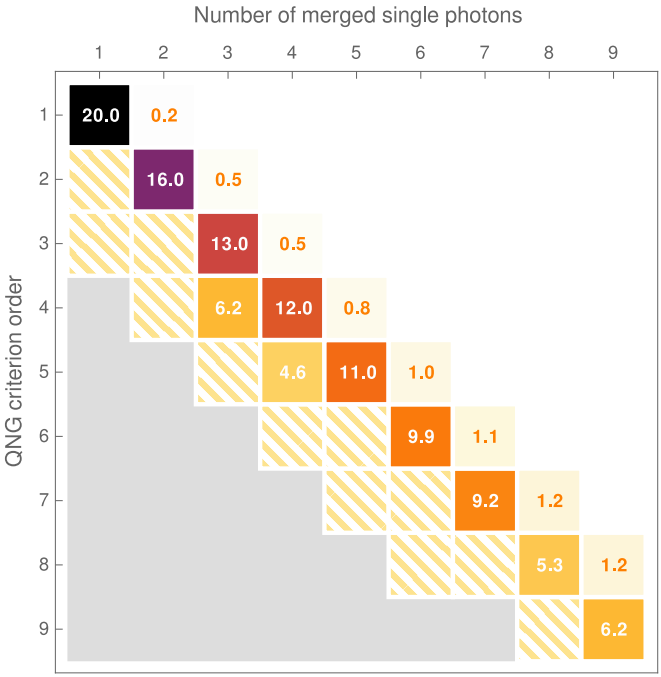

Figure 10: Table of QNG depths (in dB). The horizontal axis shows the number of single-photon states that comprise the measured state. The vertical axis represents the order of the QNG criterion used to measure the state (n in equation (12)). The diagonal represents the data being shown in Figure 9. Solid-colored tiles represent points with positively measured QNG despite statistical uncertainties. For points above the diagonal, the depth estimates are conservative and lower than the actual QNG depth, because R_{n+1} is no longer caused solely by noise. The upper white region represents combinations of measured states and criteria that did not show QNG. Orange stripes denote measurements where statistical uncertainty intersects with the QNG criterion border, making the result inconclusive. Data in the grey region contain no detections at all.

taken into account, which was $\approx$ 50%. However, no correction has been done in the data, and the results represent direct witnessing of QNG using a lossy detector. In this regime, witnessing the negativity of the Wigner function would not be possible.

The measured states are very robust against optical loss, withstanding up to 5-20 dB of attenuation before their QNG character becomes undetectable. In previous work, it was demonstrated that this QNG depth can be precisely predicted.[A1]

In Figure 10, QNG depths of various multi-photon states are shown, as measured using multiple QNG criteria. Here, each multi-photon state is positively detected with at least one order of the QNG criterion.

6 Genuine QNG

This section summarizes the results reported by Lachman, Straka, and colleagues (2018)[A4].

The proposed *genuine* n-photon quantum non-Gaussianity – GQNG(n) – represents a hierarchy of quantum properties that rule out any mixtures of Gaussian-transformed superpositions of Fock states up to $n-1$.[A4] Namely, the property of the n^{th} order states that $\rho_n \neq \int P(\psi_n)\,|\psi_n\rangle\langle\psi_n|$, where $|\psi_n\rangle = S(\xi)D(\alpha)\sum_{k=0}^{n-1} c_k\,|k\rangle$.

Using the detection approach from section 5, sufficient criteria were formulated for GQNG as well by Lachman and Filip.[A4] They can be found numerically, while for low number of photons the approximation of the n^{th} order reads[A4]

$$R_{n+1} \lesssim \frac{(1+n)^{2n}(2+n)^2(1+n)!R_n^3}{18n^2(n!)^3}. \tag{13}$$

To witness this property, a multi-mode approach based on SPDC was used, as described in section 5. In addition, the sensitivity of genuine QNG to incoherently added noise was explored, which was supplied by an external laser diode. The schematic of the measurement is depicted in Figure 11.

The results shown in Figure 12 exhibit genuine QNG up to order $n = 3$. This was achieved by reducing SPDC gain (pump power) to a point where multiphoton contributions are sufficiently low, but the overall rate allows measuring statistically significant results over the course of a few hours.

The results also provide an insight of how other multiphoton states fare in criteria that do not correspond to their heralded number of photons. In the data, only states with the number of photons higher than the order of the criterion provided statistically significant results. All of these states (numbered points in Figure 12) are located outside the genuine QNG witness region.

The results additionally show the effect of an incoherently added noise. In a communication line, such noise could be coupled from external sources and would decrease the recognizability of quantum properties. The noise signal was provided by an attenuated laser diode coupled by an imbalanced beam splitter into the experiment. By controlling the intensity, the portion of additional noise was varied, resulting in a shift along the vertical axis in Figure 12. The shift of the points in the horizontal axis is caused by unwanted back-reflections in the optical setup resulting in noise leakage into the heralding arm.

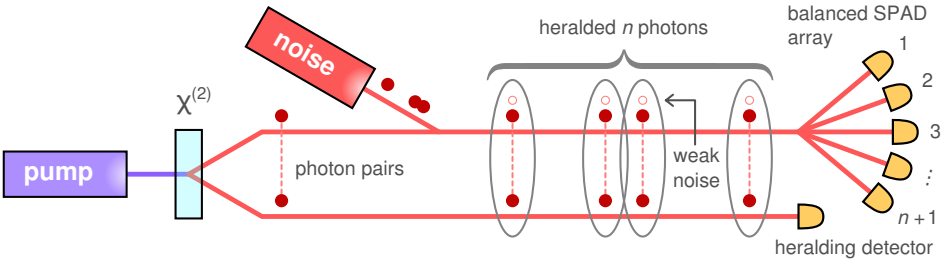

Figure 11: A schematic of the measurement. Temporally correlated photon pairs are produced by SPDC in a nonlinear crystal. An attenuated laser beam is incoherently mixed into one of the arms and serves as a source of excess noise. n time windows with heralded single photons are collected and measured on a balanced multichannel detector.

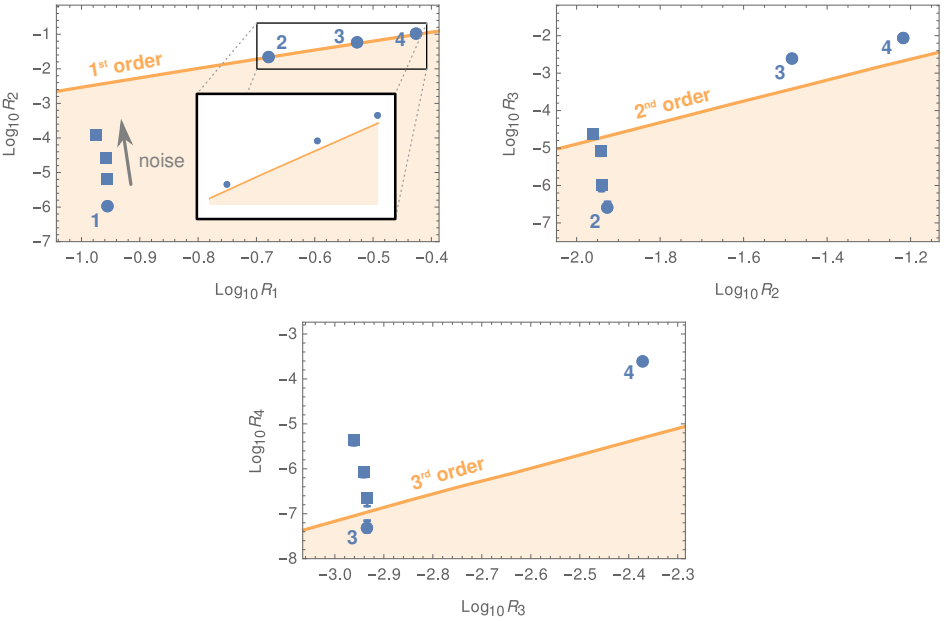

Figure 12: Data measured for various number of heralded photons (blue circles) with respect to three orders of genuine QNG (orange regions). All points were measured with identical SPDC parameters, meaning identical single-photon states that constituted the multiphoton states. Estimated depth of genuine QNG for 1–3 heralded photons are respectively 36 dB, 6.3 dB and 0.6 dB. Square points represent added Poissonian noise with mean number of photons $\overline{n} = 4 \times 10^{-5}$, 2×10^{-4}, 1×10^{-3}.

7 Generating arbitrary classical photon statistics

This chapter is based on the publication by Straka and colleagues (2018).[A3]

The following work introduces a device based on acousto-optical modulation that can be programmed to perform arbitrary intensity modulation. This can be used as a source of light with programmable photon statistics and also for simulation of transmission fluctuations in communication channels.[21–24] Additionally, a new method is proposed to obtain the distribution of optical intensity from an arbitrary photon-number distribution. An experimental demonstration is given, covering several statistics including Poisson, various super-Poisson, thermal, log-normal, bimodal, and uniform distributions. The generated statistics are characterized using a time-multiplexed photon-number-resolving detector and compared with theoretical expectations. Among the demonstrated features are faithful tail behaviour of photon statistics and producing highly bunched light. The proposed generator is also readily extensible to the pulse regime or other techniques of modulation.

If a photon statistics p_n is given instead of the intensity distribution $P(W)$, Mandel's formula needs to be inverted. There are several different approaches found in the literature,[25–28] but here full inversion to this ill-posed problem is not needed. The photon statistics to be generated is always specified up to a certain $n_{\max}$. Because the number of discrete values of intensity W_i is $N_W = 128$ in the experiment, Mandel's formula becomes a linear matrix transformation

$$\sum_{i=1}^{N_W} A_{ni} P_i = p_n \tag{14}$$

with $P_i = P(W_i)$ being the probability vector and $A_{ni} = e^{-W_i} W_i^n / n!$ a known transformation matrix. If the right side p_n is given, the task is to find the solution vector P_i. Considering normalization, the problem has a form

$$\begin{pmatrix} A_{0,1} & \cdots & A_{0,N_W} \\ \vdots & \ddots & \vdots \\ A_{n_{\max},1} & \cdots & A_{n_{\max},N_W} \\ 1 & \cdots & 1 \end{pmatrix} \begin{pmatrix} P_1 \\ P_2 \\ \vdots \\ P_{N_W} \end{pmatrix} = \begin{pmatrix} p_0 \\ p_1 \\ \vdots \\ p_{n_{\max}} \\ 1 \end{pmatrix}, \; P_i \geq 0 \; \forall i. \tag{15}$$

To avoid the ambiguity of defining a metric, only precise solutions are considered. In practical terms, this means an upper limit on $n_{\max}$ and classical photon statistics. In order to solve a linear system, a Python-implemented non-negative least squares (NNLS) algorithm was used, as published by Lawson and Hanson.[B4] This proved to be an efficient method of finding a precise solution. When defining the photon statistics, $n_{\max}$ was always kept sufficiently low and $W_{\max}$ chosen such that the solution would

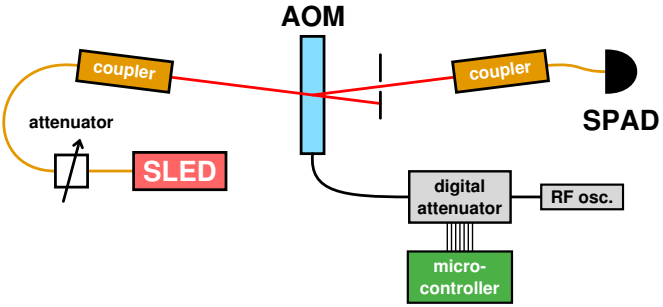

Figure 13: The scheme of the generator. Light from a superluminescent diode (SLED) is sent through an acousto-optical modulator (AOM), and the first diffraction order is coupled into a single-mode fibre and detected on a silicon single-photon avalanche diode (SPAD). The AOM is fed from a harmonic signal generator through a programmable attenuator with a parallel 7-bit interface connected to a microcontroller board.

be exact within machine precision. Because the matrix rank is $n_{\max} + 2$, the solution vector P_i typically exhibits the same number of non-zero elements.

The experimental setup (see Figure 13) employed a superluminescent diode due to its long-term power stability better than 10^{-4} (QPhotonics QSDM-810-2). It was centred around 810 nm and coupled to a single-mode fibre. Light was decoupled into free space and sent through an AOM (Brimrose TEM-125-10-800). The first diffraction order was collected into a single-mode fibre and measured. The AOM was driven by a 125-MHz harmonic signal generated in a harmonic signal generator and passed through a digital step attenuator (Mini-Circuits ZX76-31R75PP+). The attenuator was controlled by an ARM microcontroller (Arduino Due) through a 7-bit parallel interface.[29] There were 128 attenuation levels separated by 0.25 dB with a switching speed below 0.5 µs. The specified responses are 300 ns for the attenuator and 150 ns for the AOM. The diffracted optical intensity was approximately linear with respect to the RF signal power.

Detection was performed by a silicon single-photon avalanche diode (SPAD, Excelitas SPCM CD3543H). The width of the detection window T was 10 µs, which is much larger than the recovery time of the SPAD (23 ns), so that the SPAD can distinguish the number of photons incident during the detection window. Data were collected using an electronic time-to-digital converter with a timing resolution of 156 ps (UQDevices UQD-Logic-16).

The intensity modulation was a stepwise sequence of intensity levels and fully controlled by the microcontroller. The sequence was random with a user-specified statistical distribution implemented by an integrated hardware random number generator. The modulation period was 1 ms, which is much longer than the detection window. Together with fast level switching, the optical intensity in each detection window can be considered constant so that the response of the detector can be modelled. The overall

model of the data is then a statistical mixture of constant-intensity models with weights specified by P_i, just like the intensity itself.

The detection model has to take into account all relevant imperfections of the detector.[B1] Some have no impact on the measurement. Finite detection efficiency is simply included in the overall attenuation. Background counts are very low and contribute to an offset in intensity, which is accounted for in calibration. However, the effects of recovery time and afterpulsing have a measurable effect on the detected photon statistics. The model used here is discussed in section 3.

All of these effects can be measured, simulated for each intensity W_i and the result compared to measured data. It was found that for constant intensities (Poisson light), the measured photon statistics differs from the predicted model by less than $6 \cdot 10^{-4}$ for each p_n. All of the data that use NNLS inversion have accuracy comparable to this systematic error. Figures 14 and 15 present various generated photon statistics.

One approach is to take a specified photon statistics p_n and perform the NNLS inversion to obtain an intensity distribution. This inversion-approach is universal and does not require any prior knowledge or decomposition of $P(W)$. The other method (intensity-approach) is simply implementing a given intensity distribution. In that case, both limited dynamic range and finite sampling need to be accounted for. The data show that both approaches can lead to accurate results (see Figures 14, 15 and Table 1).

For the measured data, the accuracy of the generated photon statistics needs to be evaluated. A detection model is employed that arises from the intensity statistics $P(W)$ and models the SPAD response to any intensity W. If $P(W)$ was obtained by the inversion-approach, which provides exact solutions up to $n_{\max}$, accurate photon statistics is expected only up to $n_{\max}$. Beyond that, high accuracy of the model is achieved if the photons statistics has already been covered enough, that is if $\sum_{n=0}^{n_{\max}} p_n \to 1$.

To show the difference between model and data, individual differences δp_n are plotted in Figures 14 and 15. For quantification of the overall difference between the two probability distributions, a very conservative definition was chosen: total-variation distance Δ. It is defined as the maximum difference between probabilities of any possible set of samples $\{n\} \subseteq \mathbb{N}^0$. The distances for most photon statistics, and therefore maximal deviations in generated probabilities, are in the order of $\Delta \sim 10^{-3}$ (see Table 1).

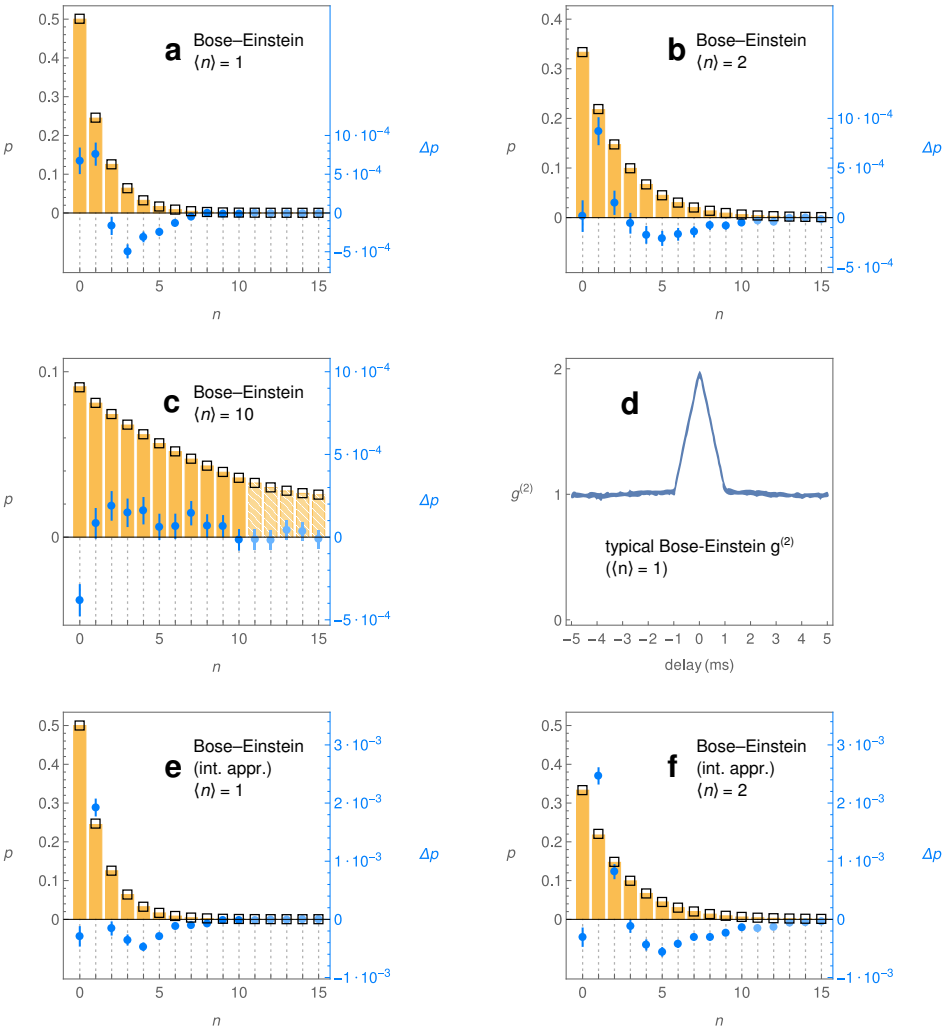

Figure 14: Generated Bose-Einstein statistics. Additional information in Table 1. Orange bars represent the expected model. Note that the model is not strictly equal to theoretical p_n, because it includes SPAD recovery time and afterpulses. Squares represent measured data. The difference between them, $\delta p = p_{\text{data}} - p_{\text{model}}$, is represented by blue points on a magnified scale. Lighter points and striped bars represent values beyond $n_{\max}$. **a – c:** Bose-Einstein statistics. NNLS was used to calculate $P(W)$. **d:** typical shape of the autocorrelation function $g^{(2)}$. **e, f:** Bose-Einstein statistics. Intensity was modulated with negative exponential distribution.

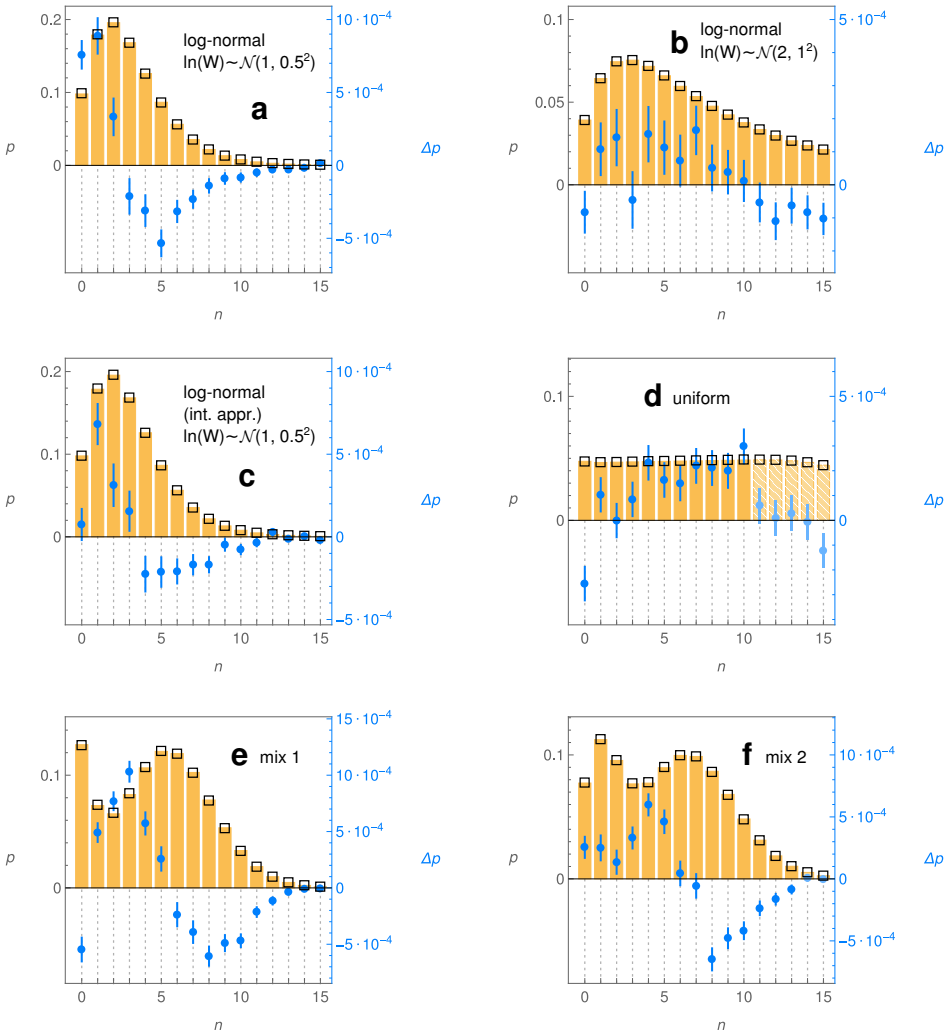

Figure 15: Miscellaneous generated photon statistics (continuing from Figure 14). Additional information in Table 1. For brevity, a normally distributed variable X with mean X_0 and variance σ^2 is denoted as $X \sim \mathcal{N}(X_0, \sigma^2)$. **a, b:** desired statistics are based on log-normal intensity distributions. NNLS inversion was used to calculate $P(W)$. **c:** same as **a**, but using log-normal modulation in intensity. **d:** a uniform distribution $p = 1/21$. NNLS inversion used. **e:** a mixture of 1/4 Bose-Einstein statistics with $\langle n \rangle = 1$ and 3/4 normally convoluted Poisson statistics ($W \sim \mathcal{N}(6, 0.5^2)$). NNLS inversion used. **f:** a mixture of two convoluted Poisson statistics, $W \sim 2/3\, \mathcal{N}(1.5, 0.25^2) + 1/3\, \mathcal{N}(7, 0.25^2)$. NNLS inversion used.

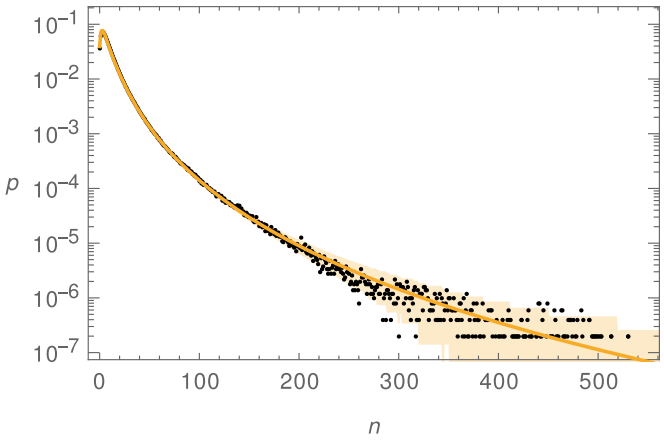

Figure 16: Measured log-normal distribution log-$\mathcal{N}(2, 1^2)$ with pronounced heavy-tailed behaviour. Black points denote experimental data and the orange curve is the theoretical expectation. Orange area denotes statistical confidence region of 2σ, so approximately 95 % of all data should be within. For this measurement, the modulation period was 2 ms. The detection window was extended to 200 µs to avoid detector saturation for high photon numbers. Measurement time was 1000 s.

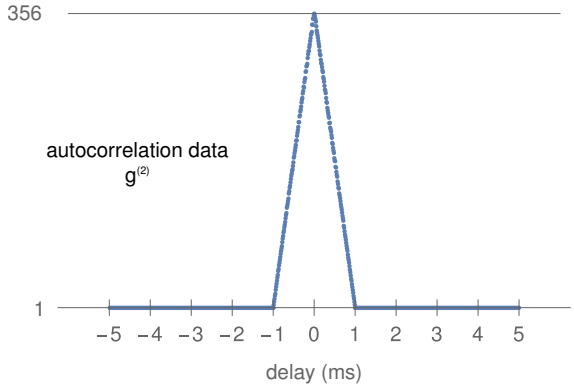

Figure 17: The maximum measured autocorrelation value that is achievable using the device in its present form; the result of a two-detector coincidence measurement. Blue curve represents data for a coincidence window of 10 ns, delay values were sampled by 10 µs and the uncertainty is lower than the thickness of the curve. The shape corresponds to stepwise intensity modulation with 1-ms period. The signal was a random mixture of two intensities with count rates on each detector approximately 3 Mcps (probability $p = 6.6 \cdot 10^{-4}$) and 2 kcps (probability $1 - p$). The intensities were chosen such that dark counts and recovery time of the detector would have the smallest effect on the superbunching.

statistics	quantity	$n_{\max}$	$W_{\max}$	Δ [$\times 10^{-3}$]
B–E(1)	n	10	15	1.4
B–E(1)	W	–	13	1.9
B–E(2)	n	10	15	1.0
B–E(2)	W	–	20	3.3
B–E(10)	n	10	20	0.6
log-$\mathcal{N}(1, 0.5^2)$	n	15	20	2.0
log-$\mathcal{N}(1, 0.5^2)$	W	–	30	1.3
log-$\mathcal{N}(2, 1^2)$	n	15	30	1.4
log-$\mathcal{N}(2, 1^2)$	W	–	500	14.7
$\frac{1}{4}$B–E(1) + $\frac{3}{4}\mathcal{N}(6, 0.5^2)$	n	15	15	3.1
$\frac{1}{3}\mathcal{N}(1.5, 0.25^2) + \frac{2}{3}\mathcal{N}(7, 0.25^2)$	n	13	15	2.1
uniform(0, 20)	n	10	20	1.9

Table 1: Results for generated photon statistics. Data shown in Figs. 14, 15 and 16. Quantity denotes the physical quantity specified. For number of photons n, NNLS inversion was used to obtain $P(W)$, and for intensity W, distribution $P(W)$ was given directly. $n_{\max}$ represents the upper limit on the given probability space and $W_{\max}$ is the maximum intensity. Δ is the total-variation distance. Definitions of statistical notations follow. B–E($\langle n \rangle$): Bose–Einstein photon statistics or negative exponential intensity distribution, where $\langle n \rangle = \langle W \rangle$. $\mathcal{N}(\langle W \rangle, \sigma^2)$: normally distributed intensity with mean $\langle W \rangle$ and variance σ^2, or the corresponding photon statistics. log-$\mathcal{N}(\langle \ln W \rangle, \sigma^2)$: log-normal distribution of intensity or the corresponding photon statistics. The moment parameters are the same as for the normal distribution, except here they pertain to $\ln(W)$. uniform(n_1,n_2): uniform photon statistics $p_n = 1/(n_2 - n_1 + 1)$ for $n_1 \leq n \leq n_2$.

8 Conclusion

The thesis covers generation of photonic quantum states in two main areas: producing a heralded number of photons and generating arbitrary photon statistics. The results furthermore address detection and characterization of the photonic states by witnessing quantum non-Gaussianity, verifying generated photon statistics and modelling the counting response of single-photon avalanche diodes.

First, multiple single-photon sources were subjected to QNG analysis. The results show very different values of QNG depths among states that are all nonclassical. Although the statistical differences between single-photon states generated by various platforms are known, the results offer new insight into fundamental importance of such differences. The QNG depth offers a way to quantify how resilient these states are in optical applications that involve loss. The resilience is considered in regard to QNG, which is a fundamental quantum property of all Fock states that needs to be maintained among experimentally generated states of sufficient quality. This motivation concerns multiphoton states as well. The results show that multi-mode states generated by SPDC exhibit QNG despite the systematic noise and optical losses present in both generation and detection. The detected photon statistics was found to be very similar to statistics of attenuated Fock states; the extra noise however still limited the recognizability of quantum non-Gaussian properties.

The QNG results were analyzed in terms of experimental parameters. For SPDC, continuous-wave pump was shown to produce lower multiphoton noise than pulsed. There is also an optimal heralding time window maximizing QNG depth that depends on detector characteristics. When compared to a quantum dot, SPDC can generate much more robust states at present, but its noise is fundamentally unavoidable. Additionally, reducing the noise simultaneously reduces the generation rate. Quantum dots are not limited by this trade-off and further improvement of the technical aspects of quantum dot sources could lead to single-photon states more robust than those generated by SPDC.

Heralded multiphoton states were also shown to exhibit genuine n-photon quantum non-Gaussianity, which is tied to a certain maximum number of photons enveloped by Gaussian transformations. Although these states might possess positive Wigner function due to excess optical loss, they exhibit quantum properties that actually go beyond the negativity of the Wigner function. In fact, the presented methodology is capable of recognizing very subtle differences that distinguish vastly dissimilar quantum states like attenuated Fock states $|n\rangle$ and $(n-1)$-photon Gaussian mixtures.

The thesis furthermore presented a generator of arbitrary classical photon statistics than can be fully programmed by the user. Various statistics were generated including Poissonian, super-Poissonian, thermal, and log-normal. Very high generation accuracy $\delta p_n < 10^{-3}$ was reached, which corresponds to the accuracy of the detection mechanism. An efficient inversion method was proposed to turn an arbitrary photon statistics into an optical intensity distribution. The concept of the generator can be extended to

any form of intensity modulation with possible increases in speed and range of generated statistics by orders of magnitude. The generator can also be straightforwardly used in a pulsed regime to produce single-mode states with given statistics. Another use is stochastic loss modulation to simulate realistic transmission channels. As an experimental advance, the proposed method of modulation is capable of putting out bunched light with much higher intensity than the conventional rotating glass approach.

In the course of solving these projects, experimental methods were developed and described in sections 2 and 3. A source of correlated photon pairs was constructed, characterized and used for the QNG measurements. The counting response of silicon single-photon avalanche diodes was theoretically modelled both analytically and in simulation.

In conclusion, the presented results contribute to methods of generating and characterizing both non-classical and classical light. QNG and genuine QNG witnessing can aid with experimental development of single- and multiphoton sources, where the current state-of-the-art easily satisfies nonclassicality, but is still significantly limited in terms of the Wigner function negativity. The arbitrary-photon-statistics methodology currently represents the most accurate and tunable engineering of photon statistics and can be used to simulate communication channels, calibrate the response of photon-number-resolving detectors, or probe physical phenomena sensitive to photon statistics. The SPAD counting models extend the currently published counting models that are used to predict the measured number of detections as a function of the incident rate. This could also advance detector calibration and inferring the properties of the optical signal based on the measured data.

References

Articles covering the presented results

A1 I. Straka, A. Predojević, T. Huber, L. Lachman, L. Butschek, M. Miková, M. Mičuda, G. S. Solomon, G. Weihs, M. Ježek, and R. Filip:
'Quantum non-Gaussian depth of single-photon states',
Physical Review Letters **113**, 223603 (2014).

A2 I. Straka, L. Lachman, J. Hloušek, M. Miková, M. Mičuda, M. Ježek, and R. Filip:
'Quantum non-Gaussian multiphoton light',
npj Quantum Information **4**, 1 (2018).

A3 I. Straka, J. Mika, and M. Ježek:
'Generator of arbitrary classical photon statistics',
Optics Express **26**, 8998–9010 (2018).

A4 L. Lachman, I. Straka, J. Hloušek, M. Ježek, and R. Filip:
'Faithful hierarchy of genuine n-photon quantum non-Gaussian light',
arXiv:1810.02546 (2018).

Books

B1 A. Migdall, S. V. Polyakov, J. Fan, and J. C. Bienfang:
Single-photon generation and detection,
(Academic Press, 2013).

B2 D. L. Snyder and M. I. Miller:
Random point processes in time and space,
(Springer-Verlag New York, 1991).

B3 D. F. Walls and G. J. Milburn:
Quantum optics,
Second Edition (Springer-Verlag, 2008).

B4 C. Lawson and R. Hanson:
Solving least squares problems,
Classics in Applied Mathematics (Society for Industrial and Applied Mathematics, 1995).

Articles, proceedings and theses

1 I. Straka:
'Optical frequency conversion and non-classical light generation',
master's thesis (Faculty of Science, Palacký University, Olomouc, 2012).

2 M. Ježek, I. Straka, M. Mičuda, M. Dušek, J. Fiurášek, and R. Filip:
'Experimental test of the quantum non-Gaussian character of a heralded single-photon state',
Physical Review Letters **107**, 213602 (2011).

3 J. Mika:
'Preparing arbitrary statistics of light by intensity modulation',
master's thesis (Faculty of Science, Palacký University, Olomouc, 2017).

4 M. Neset:
'Design and characterization of entangled photon sources', Czech,
bachelor's thesis (Faculty of Science, Palacký University, Olomouc, 2018).

5 C. K. Hong, Z. Y. Ou, and L. Mandel:
'Measurement of subpicosecond time intervals between two photons by interference',
Physical Review Letters **59**, 2044–2046 (1987).

6 J. W. Müller:
'Dead-time problems',
Nuclear Instruments and Methods **112**, 47–57 (1973).

7 R. J. Glauber:
'Coherent and incoherent states of the radiation field',
Physical Review **131**, 2766–2788 (1963).

8 H. J. Kimble, M. Dagenais, and L. Mandel:
'Photon antibunching in resonance fluorescence',
Physical Review Letters **39**, 691–695 (1977).

9 R. Filip and L. Mišta:
'Detecting quantum states with a positive Wigner function beyond mixtures of Gaussian states',
Physical Review Letters **106**, 200401 (2011).

10 M. G. Genoni, M. L. Palma, T. Tufarelli, S. Olivares, M. S. Kim, and M. G. A. Paris:
'Detecting quantum non-Gaussianity via the Wigner function',
Physical Review A **87**, 062104 (2013).

11 C. Hughes, M. G. Genoni, T. Tufarelli, M. G. A. Paris, and M. S. Kim:
'Quantum non-Gaussianity witnesses in phase space',
Physical Review A **90**, 013810 (2014).

12 J. Park and H. Nha:
'Demonstrating nonclassicality and non-Gaussianity of single-mode fields: Bell-type tests using generalized phase-space distributions',
Physical Review A **92**, 062134 (2015).

13 B. Kühn and W. Vogel:
'Quantum non-Gaussianity and quantification of nonclassicality',
Physical Review A **97**, 053823 (2018).

14 M. Ježek, A. Tipsmark, R. Dong, J. Fiurášek, L. Mišta, R. Filip, and U. L. Andersen:
'Experimental test of the strongly nonclassical character of a noisy squeezed single-photon state',
Physical Review A **86**, 043813 (2012).

15 A. Predojević, M. Ježek, T. Huber, H. Jayakumar, T. Kauten, G. S. Solomon, R. Filip, and G. Weihs:
'Efficiency vs. multi-photon contribution test for quantum dots',
Optics Express **22**, 4789–4798 (2014).

16 C. Baune, A. Schönbeck, A. Samblowski, J. Fiurášek, and R. Schnabel:
'Quantum non-Gaussianity of frequency up-converted single photons',
Optics Express **22**, 22808–22816 (2014).

17 L. Lachman and R. Filip:
'Robustness of quantum nonclassicality and non-Gaussianity of single-photon states in attenuating channels',
Physical Review A **88**, 063841 (2013).

18 R. Filip and L. Lachman:
'Hierarchy of feasible nonclassicality criteria for sources of photons',
Physical Review A **88**, 043827 (2013).

19 A. Predojević, S. Grabher, and G. Weihs:
'Pulsed Sagnac source of polarization entangled photon pairs',
Optics Express **20**, 25022–25029 (2012).

20 H. Jayakumar, A. Predojević, T. Huber, T. Kauten, G. S. Solomon, and G. Weihs:
'Deterministic photon pairs and coherent optical control of a single quantum dot',
Physical Review Letters **110**, 135505 (2013).

21 I. Capraro, A. Tomaello, A. Dall'Arche, F. Gerlin, R. Ursin, G. Vallone, and P. Villoresi:
'Impact of turbulence in long range quantum and classical communications',
Physical Review Letters **109**, 200502 (2012).

22 V. C. Usenko, B. Heim, C. Peuntinger, C. Wittmann, C. Marquardt, G. Leuchs, and R. Filip:
'Entanglement of Gaussian states and the applicability to quantum key distribution over fading channels',
New Journal of Physics **14**, 093048 (2012).

23 D. Vasylyev, A. A. Semenov, and W. Vogel:
'Atmospheric quantum channels with weak and strong turbulence',
Physical Review Letters **117**, 090501 (2016).

24 M. Bohmann, R. Kruse, J. Sperling, C. Silberhorn, and W. Vogel:
'Probing free-space quantum channels with laboratory-based experiments',
Physical Review A **95**, 063801 (2017).

25 G. Bédard:
'Analysis of light fluctuations from photon counting statistics',
Journal of the Optical Society of America **57**, 1201 (1967).

26 J. Peřina and L. Mišta:
'Reformulation of the optical equivalence theorem in terms of the Laguerre polynomials',
Annalen der Physik **477**, 372–382 (1969).

27 C. Byrne, D. Haughton, and T. Jiang:
'High-resolution inversion of the discrete Poisson and binomial transformations',
Inverse Problems **9**, 39 (1993).

28 J. C. Earnshaw and D. Haughey:
'Inversion of the Poisson transform using proportionally spaced cubic B-splines',
Review of Scientific Instruments **67**, 4387–4391 (1996).

29 R. Hošák and M. Ježek:
'Arbitrary digital pulse sequence generator with delay-loop timing',
Review of Scientific Instruments **89**, 045103 (2018).

List of publications

First-author publications in impacted journals and works that cite them according to the Web of Science

i I. Straka, A. Predojević, T. Huber, L. Lachman, L. Butschek, M. Miková, M. Mičuda, G. S. Solomon, G. Weihs, M. Ježek, and R. Filip: 'Quantum Non-Gaussian Depth of Single-Photon States', Physical Review Letters **113**, 223603 (2014).

- S. Xiang, X. Zhu, and K. Song: 'Non-Gaussianity dynamics of two-mode squeezed number states subject to different types of noise based on cumulant theory', CHINESE PHYSICS B **27**, 100305 (2018).
- K. Stensson and G. Bjork: 'Measurement of the two-time intensity-correlation function of arbitrary states', PHYSICAL REVIEW A **98**, 033812 (2018).
- B. Kuehn and W. Vogel: 'Quantum non-Gaussianity and quantification of nonclassicality', PHYSICAL REVIEW A **97**, 053823 (2018).
- L. Schweickert, K. D. Jons, K. D. Zeuner, S. F. C. da Silva, H. Huang, T. Lettner, M. Reindl, J. Zichi, R. Trotta, A. Rastelli, and V. Zwiller: 'On-demand generation of background-free single photons from a solid-state source', APPLIED PHYSICS LETTERS **112**, 093106 (2018).
- L. Happ, M. A. Efremov, H. Nha, and W. P. Schleich: 'Sufficient condition for a quantum state to be genuinely quantum non-Gaussian', NEW JOURNAL OF PHYSICS **20**, 023046 (2018).
- I. Straka, L. Lachman, J. Hlousek, M. Mikova, M. Micuda, M. Jezek, and R. Filip: 'Quantum non-Gaussian multiphoton light', NPJ QUANTUM INFORMATION **4**, 4 (2018).
- H. Nha, J. Lee, and J. Park: 'Nonclassicality and entanglement for continuous-variable quantum information', in QUANTUM AND NONLINEAR OPTICS V, Vol. 10825, edited by Gong, Q and Guo, GC and Ham, BS, Proceedings of SPIE, Conference on Quantum and Nonlinear Optics V, Beijing, PEOPLES R CHINA, OCT 11-13, 2018 (SPIE; Chinese Opt Soc, 2018).
- J. Park, J. Lee, S.-W. Ji, and H. Nha: 'Quantifying non-Gaussianity of quantum-state correlation', PHYSICAL REVIEW A **96**, 052324 (2017).
- M. Lasota, R. Filip, and V. C. Usenko: 'Sufficiency of quantum non-Gaussianity for discrete-variable quantum key distribution over noisy channels', PHYSICAL REVIEW A **96**, 012301 (2017).
- A. A. Rakhubovsky and R. Filip: 'Photon-phonon-photon transfer in optomechanics', SCIENTIFIC REPORTS **7**, 46764 (2017).

- J. Park, Y. Lu, J. Lee, Y. Shen, K. Zhang, S. Zhang, M. S. Zubairy, K. Kim, and H. Nha:
'Revealing nonclassicality beyond Gaussian states via a single marginal distribution',
PROCEEDINGS OF THE NATIONAL ACADEMY OF SCIENCES OF THE UNITED STATES OF AMERICA **114**, 891–896 (2017).
- L. Lachman and R. Filip:
'Quantum non-Gaussianity from a large ensemble of single photon emitters',
OPTICS EXPRESS **24**, 27352–27359 (2016).
- D. B. Higginbottom, L. Slodicka, G. Araneda, L. Lachman, R. Filip, M. Hennrich, and R. Blatt:
'Pure single photons from a trapped atom source',
NEW JOURNAL OF PHYSICS **18**, 093038 (2016).
- T. Huber, A. Predojevic, G. S. Solomon, and G. Weihs:
'Effects of photo-neutralization on the emission properties of quantum dots',
OPTICS EXPRESS **24**, 21794–21801 (2016).
- L. Lachman, L. Slodicka, and R. Filip:
'Nonclassical light from a large number of independent single-photon emitters',
SCIENTIFIC REPORTS **6**, 19760 (2016).
- J. Park and H. Nha:
'Demonstrating nonclassicality and non-Gaussianity of single-mode fields: Bell-type tests using generalized phase-space distributions',
PHYSICAL REVIEW A **92**, 062134 (2015).
- T. Huber, A. Predojevic, D. Foeger, G. Solomon, and G. Weihs:
'Optimal excitation conditions for indistinguishable photons from quantum dots',
NEW JOURNAL OF PHYSICS **17**, 123025 (2015).
- J. Fiurasek, C. Baune, A. Schonbeck, and R. Schnabel:
'Analysis of counting measurements on narrowband frequency up-converted single photons and the influence of heralding detector dead time',
PHYSICAL REVIEW A **91**, 013829 (2015).
- A. Predojevic:
'Resonant Excitation and Photon Entanglement from Semiconductor Quantum Dots',
in *ENGINEERING THE ATOM-PHOTON INTERACTION: CONTROLLING FUNDAMENTAL PROCESSES WITH PHOTONS, ATOMS AND SOLIDS*, edited by Predojevic, A and Mitchell, MW, Nano-Optics and Nanophotonics (2015), 303–324.

ii I. Straka*, M. Miková*, M. Mičuda, M. Dušek, M. Ježek, and R. Filip:
'Conditional cooling limit for a quantum channel going through an incoherent environment',
Scientific Reports volume **5**, 16721 (2015).
* equal contribution

- No citations

iii I. Straka*, L. Lachman*, J. Hloušek, M. Miková, M. Mičuda, M. Ježek, and R. Filip:
'Quantum non-Gaussian multiphoton light',
npj Quantum Information **4**, 1 (2018).
* equal contribution

- M. Kumazawa, T. Sasaki, and M. koahi:
'Rigorous characterization method for photon-number statistics',
OPTICS EXPRESS **27**, 5297–5313 (2019).
- J. Weinbub and D. K. Ferry:
'Recent advances in Wigner function approaches',
APPLIED PHYSICS REVIEWS **5**, 041104 (2018).
- K. Stensson and G. Bjork:
'Measurement of the two-time intensity-correlation function of arbitrary states',
PHYSICAL REVIEW A **98**, 033812 (2018).
- L. Qi, M. Manceau, A. Cavanna, F. Gumpert, L. Carbone, M. de Vittorio, A. Bramati, E. Giacobino, L. Lachman, R. Filip, and M. Chekhova:
'Multiphoton nonclassical light from clusters of single-photon emitters',
NEW JOURNAL OF PHYSICS **20**, 073013 (2018).
- B. Kuehn and W. Vogel:
'Quantum non-Gaussianity and quantification of nonclassicality',
PHYSICAL REVIEW A **97**, 053823 (2018).
- L. Happ, M. A. Efremov, H. Nha, and W. P. Schleich:
'Sufficient condition for a quantum state to be genuinely quantum non-Gaussian',
NEW JOURNAL OF PHYSICS **20**, 023046 (2018).

iv I. Straka, J. Mika, and M. Ježek:
'Generator of arbitrary classical photon statistics',
Optics Express **26**, 8998–9010 (2018).

- Y. Zhou, S. Luo, Z. Tang, H. Zheng, H. Chen, J. Liu, F.-L. Li, and Z. Xu:
'Experimental observation of three-photon superbunching with classical light in a linear system',
JOURNAL OF THE OPTICAL SOCIETY OF AMERICA B-OPTICAL PHYSICS **36**, 96–100 (2019).
- T. Lettau, H. A. M. Leymann, B. Melcher, and J. Wiersig:
'Superthermal photon bunching in terms of simple probability distributions',
PHYSICAL REVIEW A **97**, 053835 (2018).
- R. Hosak and M. Jezek:
'Arbitrary digital pulse sequence generator with delay-loop timing',
REVIEW OF SCIENTIFIC INSTRUMENTS **89**, 045103 (2018).

Other publications in impacted journals

v R. Starek, M. Micuda, M. Mikova, I. Straka, M. Dusek, P. Marek, M. Jezek, R. Filip, and J. Fiurasek:
'Nondestructive detector for exchange symmetry of photonic qubits',
NPJ QUANTUM INFORMATION **4**, 35 (2018).

vi R. Starek, M. Mikova, I. Straka, M. Dusek, M. Jezek, J. Fiurasek, and M. Micuda:
'Experimental realization of SWAP operation on hyper-encoded qubits',
OPTICS EXPRESS **26**, 8443–8452 (2018).

vii L. Podhora, P. Obsil, I. Straka, M. Jezek, and L. Slodicka:
'Nonclassical photon pairs from warm atomic vapor using a single driving laser',
OPTICS EXPRESS **25**, 31230–31238 (2017).

viii M. Micuda, R. Starek, P. Marek, M. Mikova, I. Straka, M. Jezek, T. Tashima, S. K. Ozdemir, and M. Tame:
'Experimental characterization of a non-local convertor for quantum photonic networks',
OPTICS EXPRESS **25**, 7839–7848 (2017).

ix M. Micuda, D. Koutny, M. Mikova, I. Straka, M. Jezek, and L. Mista Jr.:
'Experimental demonstration of a fully inseparable quantum state with nonlocalizable entanglement',
SCIENTIFIC REPORTS **7**, 45045 (2017).

x R. Starek, M. Micuda, M. Mikova, I. Straka, M. Dusek, M. Jezek, and J. Fiurasek:
'Experimental investigation of a four-qubit linear-optical quantum logic circuit',
SCIENTIFIC REPORTS **6**, 33475 (2016).

xi M. Mikova, I. Straka, M. Micuda, V. Krcmarsky, M. Dusek, M. Jezek, J. Fiurasek, and R. Filip:
'Faithful conditional quantum state transfer between weakly coupled qubits',
SCIENTIFIC REPORTS **6**, 32125 (2016).

xii M. Micuda, R. Starek, I. Straka, M. Mikova, M. Sedlak, M. Jezek, and J. Fiurasek:
'Experimental replication of single-qubit quantum phase gates',
PHYSICAL REVIEW A **93**, 052318 (2016).

xiii R. Starek, M. Micuda, I. Straka, M. Mikova, M. Jezek, R. Filip, and J. Fiurasek:
'Control and enhancement of interferometric coupling between two photonic qubits',
PHYSICAL REVIEW A **93**, 042321 (2016).

xiv M. Micuda, M. Mikova, I. Straka, M. Sedlak, M. Dusek, M. Jezek, and J. Fiurasek:
'Tomographic characterization of a linear optical quantum Toffoli gate',
PHYSICAL REVIEW A **92**, 032312 (2015).

xv M. Micuda, R. Starek, I. Straka, M. Mikova, M. Dusek, M. Jezek, R. Filip, and J. Fiurasek:
'Quantum controlled-Z gate for weakly interacting qubits',
PHYSICAL REVIEW A **92**, 022341 (2015).

xvi M. Micuda, I. Straka, M. Mikova, M. Dusek, M. Jezek, J. Fiurasek, and R. Filip:
'Experimental test of robust quantum detection and restoration of a qubit',
PHYSICAL REVIEW A **92**, 012324 (2015).

xvii M. Mikova, M. Sedlak, I. Straka, M. Micuda, M. Ziman, M. Jezek, M. Dusek, and J. Fiurasek:
'Optimal entanglement-assisted discrimination of quantum measurements',
PHYSICAL REVIEW A **90**, 022317 (2014).

xviii M. Micuda, E. Dolakova, I. Straka, M. Mikova, M. Dusek, J. Fiurasek, and M. Jezek:
'Highly stable polarization independent Mach-Zehnder interferometer',
REVIEW OF SCIENTIFIC INSTRUMENTS **85**, 083103 (2014).

xix M. Jezek, M. Micuda, I. Straka, M. Mikova, M. Dusek, and J. Fiurasek:
'Orthogonalization of partly unknown quantum states',
PHYSICAL REVIEW A **89**, 042316 (2014).

xx M. Micuda, M. Sedlak, I. Straka, M. Mikova, M. Dusek, M. Jezek, and J. Fiurasek:
'Process-fidelity estimation of a linear optical quantum-controlled-Z gate: A comparative study',
PHYSICAL REVIEW A **89**, 042304 (2014).

xxi M. Micuda, M. Sedlak, I. Straka, M. Mikova, M. Dusek, M. Jezek, and J. Fiurasek:
'Efficient Experimental Estimation of Fidelity of Linear Optical Quantum Toffoli Gate',
PHYSICAL REVIEW LETTERS **111**, 160407 (2013).

xxii M. Mikova, H. Fikerova, I. Straka, M. Micuda, M. Jezek, M. Dusek, and R. Filip:
'Carrying qubits with particles whose noninformational degrees of freedom are nonfactorable',
PHYSICAL REVIEW A **87**, 042327 (2013).

xxiii M. Micuda, I. Straka, M. Mikova, M. Dusek, N. J. Cerf, J. Fiurasek, and M. Jezek: 'Noiseless Loss Suppression in Quantum Optical Communication', PHYSICAL REVIEW LETTERS **109**, 180503 (2012).

xxiv M. Mikova, H. Fikerova, I. Straka, M. Micuda, J. Fiurasek, M. Jezek, and M. Dusek: 'Increasing efficiency of a linear-optical quantum gate using electronic feed-forward', PHYSICAL REVIEW A **85**, 012305 (2012).

xxv M. Jezek, I. Straka, M. Micuda, M. Dusek, J. Fiurasek, and R. Filip: 'Experimental Test of the Quantum Non-Gaussian Character of a Heralded Single-Photon State', PHYSICAL REVIEW LETTERS **107**, 213602 (2011).

Works under peer review

xxvi J. Hloušek, M. Dudka, I. Straka, and M. Ježek: 'Accurate detection of arbitrary photon statistics', arXiv:1812.02262 (2018).

xxvii L. Lachman*, I. Straka*, J. Hloušek, M. Ježek, and R. Filip: 'Faithful hierarchy of genuine n-photon quantum non-Gaussian light', arXiv:1810.02546 (2018),
* equal contribution.

Souhrn v českém jazyce

Disertační práce předkládá výzkum v oblasti detekce kvantové negaussovskosti světla a rovněž generace obecné statistiky fotonů. Jako první jsou uvedeny výsledky srovnávající kvantově negaussovské vlastnosti jednofotonových stavů produkovaných různými fyzikálními systémy. Při analýze rozpoznatelnosti těchto vlastností vzhledem k optickým ztrátám se ukázalo, že jednofotonové stavy z různých platforem, vykazujíce shodně neklasičnost, se už diametrálně liší v negaussovskosti. Vzhledem k tomu, že obou zmíněných vlastností je nutné dosáhnout při generaci ideálního jednoho fotonu, jsou uvedené poznatky uplatnitelné ve vývoji jednofotonových zdrojů.

V další části jsou uvedeny výsledky měření kvantové negaussovskosti pro vícefotonové stavy. Tyto stavy byly generovány spojením několika jednofotonových stavů generovaných optickou frekvenční konverzí. Kvantová negaussovskost byla demonstrována až pro 9 fotonů s realistickými ztrátami a šumem, což dokazuje využitelnost metody k vývoji vícefotonových stavů.

Jako další vlastnost byla ověřena vícefotonová ryzí negaussovskost, která je schopna rozpoznat přítomnost určitého minimálního počtu fotonů i přes obálku gaussovských transformací. U této metody se ukázalo, že dokáže rozeznat stavy velmi podobných statistických vlastností, které se však diametrálně liší svým charakterem.

Disertace dále uvádí metodu programovatelné intenzitní modulace jako zdroj světla s nastavitelným klasickým rozdělením počtu fotonů. Byla navrhnuta metoda výpočtu odpovídajícího intenzitního rozdělení a generováno několik klasických fotorozdělení. Navrhovaná metoda je schopna dosáhnout vysokého dynamického rozsahu i vysoké míry shlukování. Využití může nalézt u simulace komunikačních kanálů nebo měření odezvy nelineárních systémů včetně kalibrace detektorů citlivých na statistiku dopadajícího světla.

Metody využité při řešení práce zahrnují konstrukci zdroje korelovaných fotonů, jenž byl využit pro dosažení uvedených výsledků. Dále byl vyvinut model čítací odezvy jednofotonových lavinových diod, a to v numerické simulaci i analyticky. Prezentované výsledky rozšiřují stávající modely a mohou přispět k přesnější kalibraci odezvy jednofotonových lavinových diod.